Science Advances
AAAS

advances.sciencemag.org/cgi/content/full/5/8/eaaw2897/DC1

Supplementary Materials for

Photothermally and magnetically controlled reconfiguration of polymer composites for soft robotics

Jessica A.-C. Liu, Jonathan H. Gillen, Sumeet R. Mishra, Benjamin A. Evans, Joseph B. Tracy*

*Corresponding author. Email: jbtracy@ncsu.edu

Published 2 August 2019, *Sci. Adv.* **5**, eaaw2897 (2019)
DOI: 10.1126/sciadv.aaw2897

The PDF file includes:

Other Supplementary Material for this manuscript includes the following:

(available at advances.sciencemag.org/cgi/content/full/5/8/eaaw2897/DC1)

Movie S12 (.mp4 format). Unbiased DiAPLEX snapper simulation.
Movie S13 (.mp4 format). Biased DiAPLEX snapper experiment.
Movie S14 (.mp4 format). Biased DiAPLEX snapper simulation.
Movie S15 (.mp4 format). Magnet-assisted grabber.
Movie S16 (.mp4 format). Push-through grabber.
Movie S17 (.mp4 format). Five cantilevers with elastic modulus offset by 10°C.

Supplementary Materials and Methods

Material Characterization

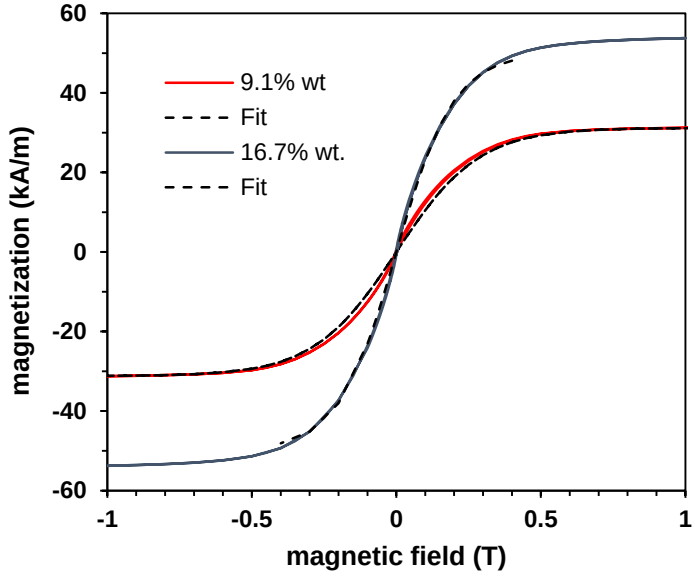

Fig. S1. Magnetization curves of loaded IROGRAN and DiAPLEX films. The field-dependent magnetization curves of IROGRAN (9.1 wt%) and DiAPLEX (16.7 wt%) films with different loadings of chained Fe microparticles were measured at 300 K. The 9.1 wt% was fit for $|B| \leq 1$ T, and the 16.7 wt% was fit for $|B| \leq 0.4$ T, which is the range provided by our permanent magnets.

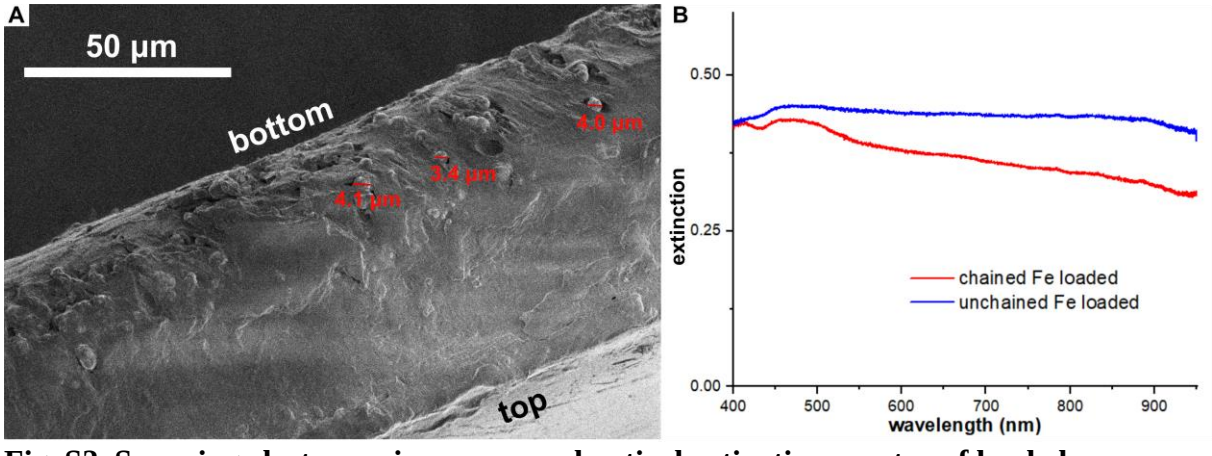

Fig. S2. Scanning electron microscopy and optical extinction spectra of loaded DiAPLEX films. (A) Scanning electron micrographs of a cross section of a DiAPLEX film with chained Fe particles (9.1 wt%) and (B) Optical extinction spectra of DiAPLEX films (~100 µm thick) with chained and unchained Fe particles (9.1 wt%).

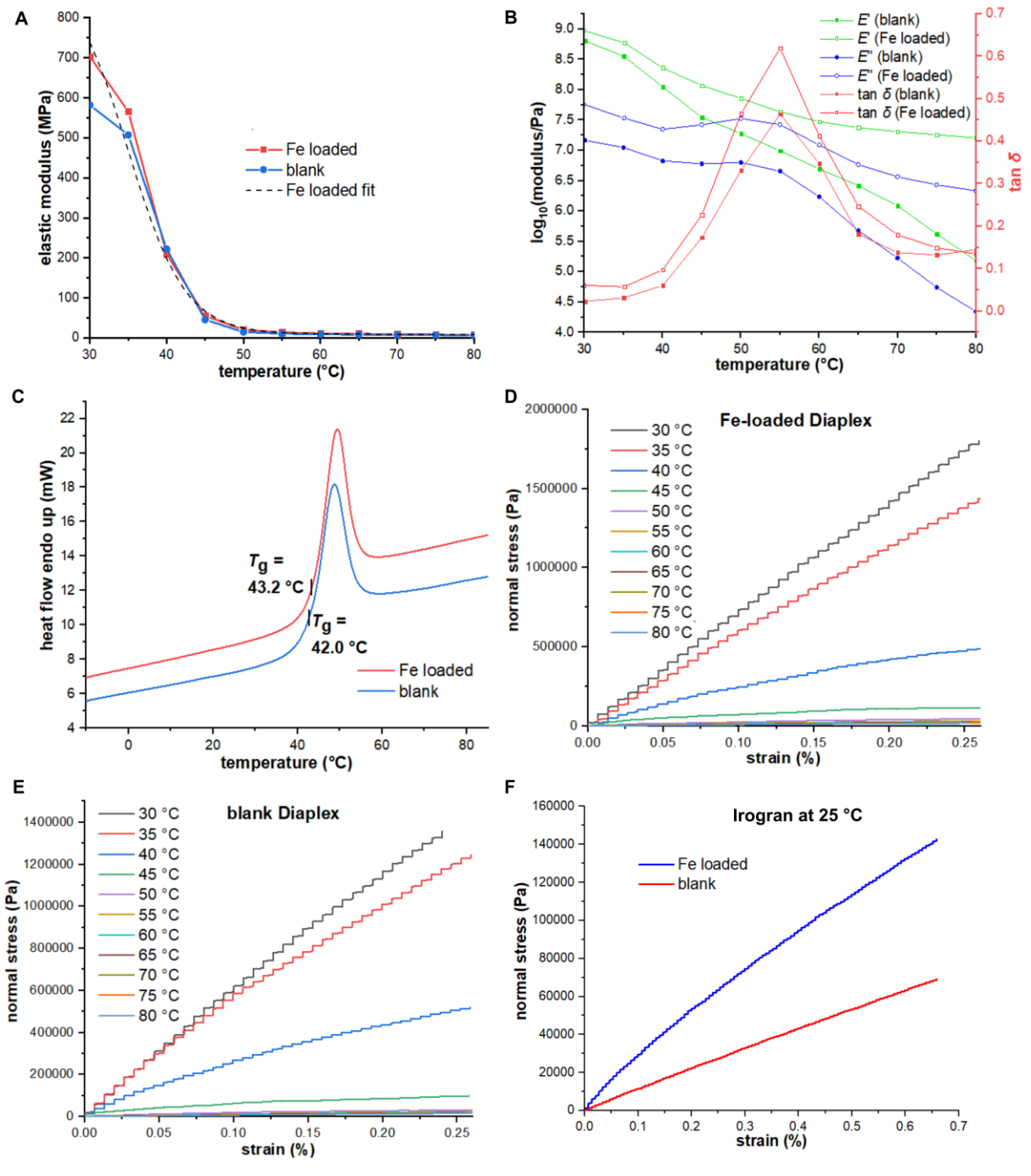

Fig. S3. Chemical and mechanical analysis of loaded and unloaded polymer films. (A) Temperature-dependent modulus of DiAPLEX films obtained from linear least-squares fitting of tensile testing curves (D,E) with a zero intercept term, including the fit $E(T)$ for the chained sample. (B) Dynamical mechanical analysis of DiAPLEX films. (C) Differential scanning calorimetry measurements of DiAPLEX samples, where T_g was obtained by extrapolating half C_P. (D,E,F) Tensile testing of (D) loaded and (E) blank DiAPLEX samples at different temperatures and (F) loaded and unloaded IROGRAN samples at 25 °C. All Fe-loaded samples contained chained Fe particles (9.1 wt%).

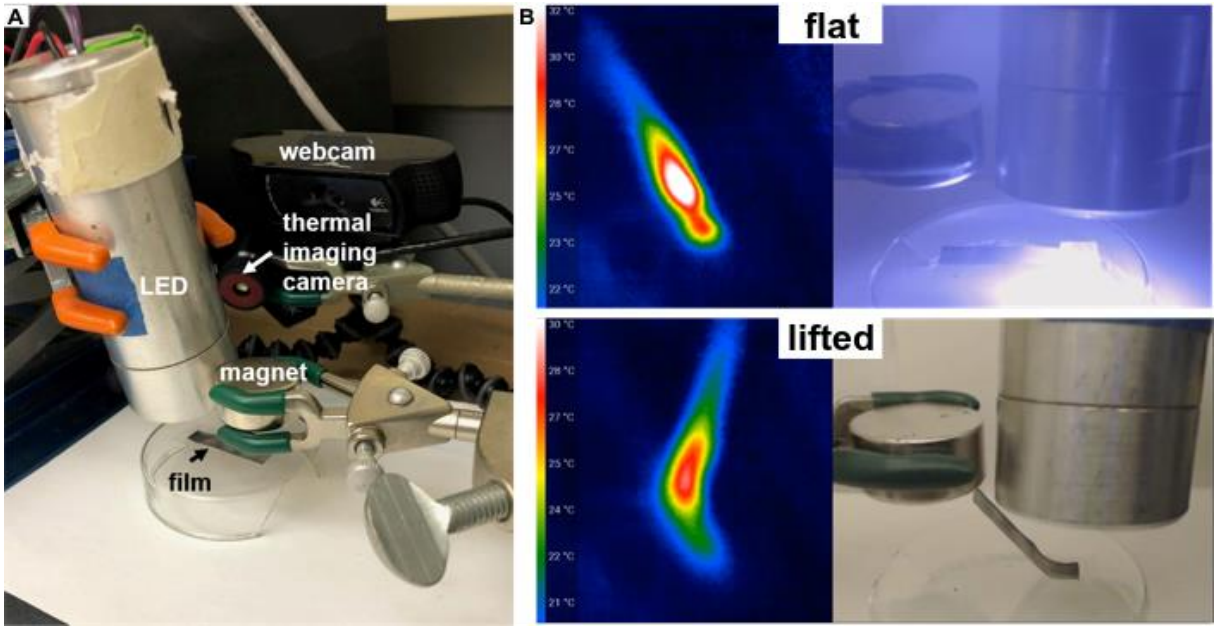

Fig. S4. Experimental setup for thermal imaging of cantilever. (A) Thermal imaging camera, webcam, LED, permanent magnet and the film are indicated in the photo. (B) Corresponding images of the film in the thermal imaging camera and webcam in flat and lifted positions. Photo Credit: Jessica A.-C. Liu, North Carolina State University.

Note About Movie S3 and the Thermal Imaging Camera

According to the manufacturer of the thermal imaging camera, there can be minor variations in the frame rate, which made it slightly out of sync with the webcam. Because the frame rate of the thermal imaging camera is not uniform over the time, minor edits were made to the thermal imaging video, either at the beginning or end of each cycle. Specifically, the thermal imaging and webcam videos were aligned based on the timing of switching on the LED in the webcam and the start of a temperature increase in the thermal imaging camera. The rate of the temperature change during actuation and lifting was not edited.

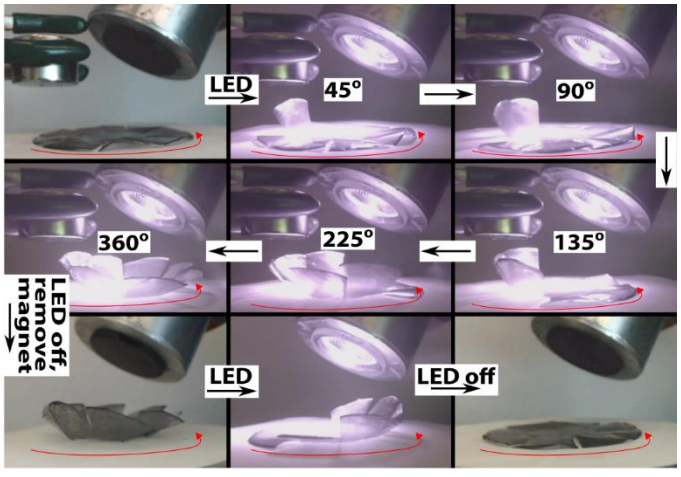

Fig. S5. DiAPLEX flower with eight petals containing unchained magnetic particles. Rotation counterclockwise beneath the LED first causes photothermal heating and softening of the petals, followed by lifting beneath the permanent magnet. Removing the magnet and turning the LED on causes the petals to return to their original, flat position. Photo Credit: Jessica A.-C. Liu, North Carolina State University.

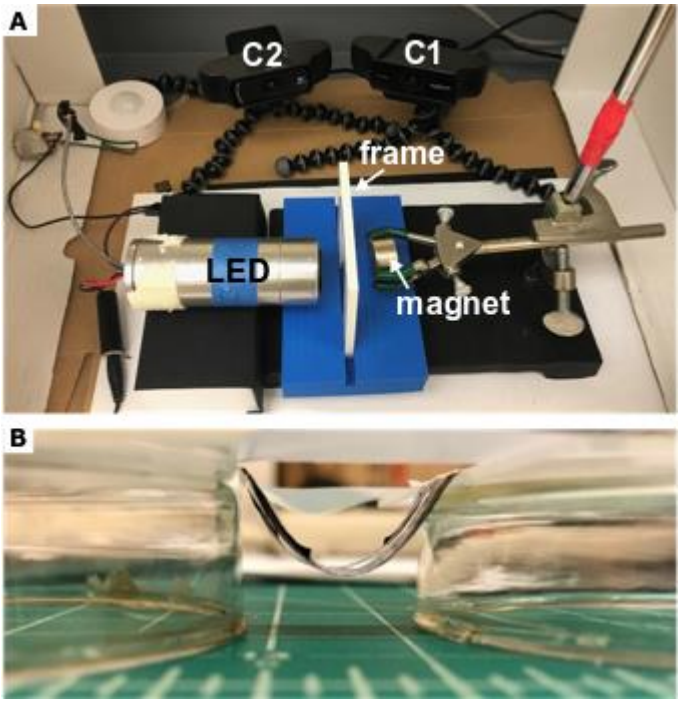

Fig. S6. Experimental setup for preparation and imaging of DiAPLEX snappers. (A) Two webcams (C1, C2), the LED, permanent magnet, and frame for supporting the snapper are indicated in the photo. (B) The polymer film was wrapped in aluminum foil, and the ends were taped to two Petri dishes, followed by heating in an oven, to prepare a biased DiAPLEX snapper. Photo Credit: Jessica A.-C. Liu, North Carolina State University.

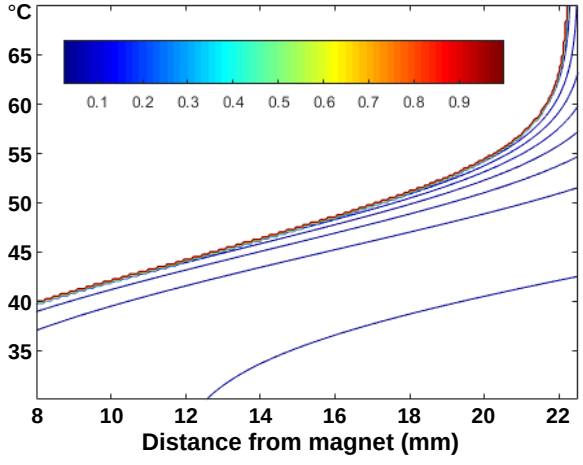

Fig. S7. Summary of simulations for an unbiased DiAPLEX snapper. A 48-mm long unbiased DiAPLEX snapper (chained, 9.1 wt% Fe loading), is cantilevered across a gap of 40 mm. The contour lines (drawn at 0.5% intervals) indicate the dependence of the degree of snapping on temperature and the distance from the magnet.

Simulation Methods

Results of the cantilever and snapper experiments were corroborated with theory by developing a numerical model of cantilever actuation. In the two-dimensional simulation, the filament is treated as a thin elastic beam comprised of 40 rigid segments along its length joined at flexible nodes. Each segment experiences a uniform magnetic field, magnetization, and magnetic field gradient according to its location relative to a simulated permanent magnet. The magnetization of the filament in the presence of a field gradient causes an attractive magnetic force on each segment, favoring displacement toward the magnet. Elastic restoring forces tend to resist displacement. Calculating the net force on each segment arising from magnetism, elasticity, and gravity allows determination of the instantaneous acceleration of the filament in any configuration (**Figure S8**). By selecting an appropriately short time interval before repeating calculation of the net force and acceleration, the dynamics of the filament can be simulated, and its equilibrium configuration can be predicted.

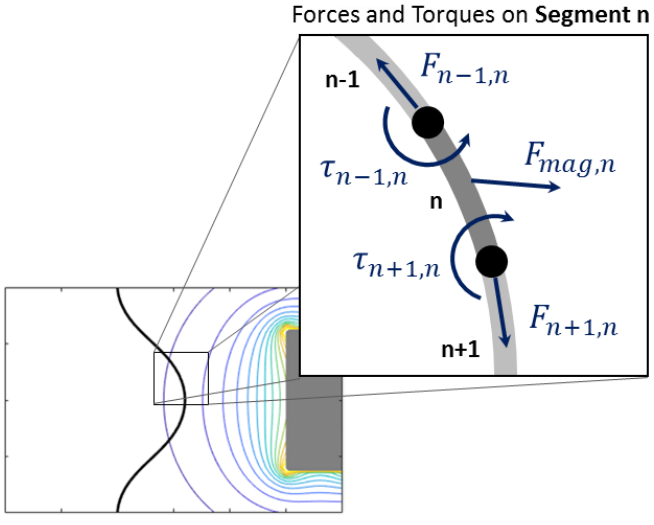

Fig. S8. Graphical representation of the net force acting on an arbitrary segment of the filament. The elastic torques (τ), elastic extension/compression forces (F), and magnetic force (F_{mag}) are depicted. Elastic forces and torques are used to find net elastic forces in x and y on each node (black circles); these are added to magnetic and gravitational forces to determine the net force on each node.

The elastic energy (U) associated with bending the filament is taken from Euler-Bernoulli theory to be

$$U = \frac{1}{2} IE \int_0^L \frac{1}{R(s)^2} ds \qquad \text{(Equation S1)}$$

where R is the radius of curvature of the beam, E is the modulus, and I is the bending moment. Assuming R is constant locally for any single segment of the filament and recognizing from geometrical considerations that $R_n = L_n / \left[2\cos\left(\theta_n / 2\right) \right]$, where θ_n is the

angle between neighboring segments and L_n is the length of a segment, then the n^{th} element of the filament experiences an elastic torque due to its neighbor, $\tau_n = dU_n / d\theta_n = IE \sin\theta_n / L_n$. For a filament of rectangular cross-section, $I = wt^3/12$, where *w* and *t* are the width and thickness of the filament, respectively. Elastic torques from nearest neighbors are added to find the net torque on each segment of the filament, then multiplied by a moment arm equal to a half-segment length to determine the force exerted on neighboring nodes. Simulations of filaments bending under the influence of gravity were compared with analytical models of beam bending and found to be in excellent agreement.

For "biased" materials that possess a curved elastic equilibrium configuration, the elastic bending torques are calculated according to the local displacement of the current configuration relative to the "relaxed" elastic equilibrium configuration; i.e., $\tau_n = IE \sin(\theta_n - \theta_{n,relaxed}) / L_n$. Shape memory polymers such as DiAPLEX are considered to possess two independent "relaxed" configurations, including a "permanent" configuration that is fixed and independent of temperature, and a "temporary" configuration with a temperature-dependent modulus that can be reset by cycling the temperature by heating to 80 °C and then cooling to room temperature. For each segment, the torques associated with displacement from the permanent and temporary equilibrium configurations are added to yield a net torque.

Elastic energy also dominates the extension and compression of the filament. The force on each segment can be described in terms of the modulus as $F = Ewt\Delta L_n / L_n$, where the restoring force *F* is in the direction opposite the extension or compression of the segment, ΔL_n. Summing the elastic bending forces due to nearest neighbors with the elastic extension and compression forces results in a two-dimensional net elastic restoring force on each node of the filament. Using elastic forces as described above to simulate the deflection of the filament under gravitational forces results in excellent agreement with analytical models of beam bending.

The magnetic field is taken to be that of an ideal cylindrical magnet and is modeled in a plane bisecting the magnet along its axis using an established algorithm (60). Each segment of the filament then attains a net volume magnetization *M* according to the local field magnitude *B*, where the magnetization curve of the IROGRAN and DiAPLEX films, *M*(*B*), has been determined via SQUID magnetometry (**Figure S1**). The energy of a dipole in a magnetic field is given by the Zeeman energy, $U = -\vec{m} \cdot \vec{B}$. Assuming any misalignment between the moment and the field is negligible, then $U = -mB = -VMB$, where the volume magnetization *M* (A/m) is in general a function of the magnetic flux density *B* (T), and *B* itself is a function of *x* and *y*. The orthogonal directions *x* and *y* can otherwise be freely chosen, as long as they are in the plane of the bending behavior (**Figure S8**). *V* is the volume of the moment. The force in the *x* direction is the negative derivative of the energy with respect to *x*, $F_x = -\frac{\partial U}{\partial x} = \frac{\partial}{\partial x}\left[VM(B)B(x,y)\right] = V\left[\frac{\partial M}{\partial B}\frac{\partial B}{\partial x}B + M\frac{\partial B}{\partial x}\right]$, and so the net magnetic force due to the field gradient is $\vec{F} = [\frac{\chi}{\mu_0}B + M]V\nabla B$. Here, the dimensionless susceptibility, $\chi = \mu_0 \frac{\partial M}{\partial B}$,

and volume magnetization M are both functions of the local field magnitude $B(x,y)$, and both $\chi(B)$ and $M(B)$ are determined from magnetometry.

From fits to the magnetization curves, the magnetization and susceptibility of the 9.1% chained Fe materials (DiAPLEX cantilever, IROGRAN snappers, DiAPLEX unbiased snapper) are found to be $M(B) = 31183\tanh(3.5B)$ and $\chi(B) = 62363\mu_0 \operatorname{sech}^2(3.5B)$ for fields applied parallel to the Fe particle chains, while fits for the 16.7% chained Fe (DiAPLEX biased snapper) are $M(B) = 49893\tanh(5B)$ and $\chi(B) = 99786\mu_0 \operatorname{sech}^2(5B)$.

The temperature-dependent modulus, $E(T)$, of DiAPLEX is determined from a fit to experimental data from tensile testing (**Figure S3**), yielding $E(T) = 468 - 459 \tanh(0.135(T - 35))$ MPa. The fit is valid for 20 °C ≤ T ≤ 80 °C. To model the shape memory effect of DiAPLEX, the modulus of the permanent configuration is taken to be $E_{perm} = E(T)_{min} = E(80\ °C)$ while the modulus of the temporary configuration is assumed to comprise the remainder, $E_{temp} = E(T) - E_{perm}$.

The program, written in MatLab 2017a, progresses as follows:
1. Assume a filament of 40 equal segments (joined at "nodes") in an initial position.
2. Calculate the length, L_n, of each segment.
3. Calculate the elastic extension / compression force in x and y on each node.
4. Calculate the angle, θ_n, between adjacent segments.
5. Calculate the elastic bending force in x and y on each node.
6. Calculate the magnetic force in both x and y.
7. Calculate the gravitational force on all nodes (neglected for the snappers).
8. Set forces to zero for fixed segments (i.e., cantilevered ends).
9. Sum all the forces in x and in y.
10. Update the momentum of each node by applying the net force for a time interval

$$\Delta p = F_{net}\Delta t$$

11. Update the position of each node by allowing it to move for a time interval

$$\Delta x = (\Delta p/m)\Delta t$$

12. Return to (2) and loop until F_{net} per node is less than a preset value, typically 10^{-8}-10^{-7} N.
13. Report final position of the filament.

At Step 10, a small amount of momentum is removed from the system to dampen internal oscillations. This amount varies between 0.1% and 0.5%, and is determined by an adaptive algorithm. The time step (Δt) for each simulation is optimized through a routine that maximizes the speed of the simulation while avoiding over-steps, which would result in a rapid divergence in F_{net}. In this simulation, Δt is typically on the order of 0.1 to 1 μs.

In simulations of cantilevers, the two nodes on the fixed end of the filament are restricted by setting the net force on each to zero. In snapper simulations, on each fixed end, two nodes are similarly restricted. In both cases, the total length of the filament between restrictions (i.e., excluding fixed "end" nodes) is preserved and set to reflect experimental conditions.

Design Considerations

Elastic Torque

If we assume the curvature of a cantilever-type actuator is constant along its length at a given displacement, then we can show from geometrical arguments that the radius of curvature is given by $R = L/(2\theta)$, where L is the length of the filament and the actuation angle θ describes the arc through which the actuator is displaced from its elastic equilibrium position (**Figure S9**).

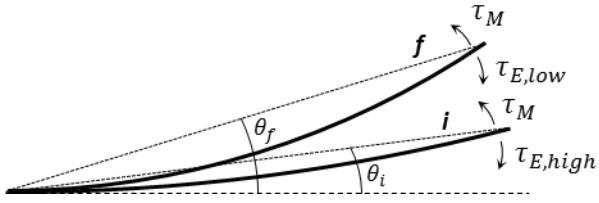

Fig. S9. Geometry of a cantilever-type SMP with constant curvature. At the initial displacement θ_i, the magnetic torque is balanced by the elastic torque at high modulus. When the material is heated, the modulus and associated elastic torque drops, resulting in a new equilibrium position at a greater displacement θ_f.

Inserting this constant R into the elastic energy (Eq. S1) and differentiating with respect to θ then yields the elastic torque on the actuator

$$\tau_E = \frac{1}{3}\frac{wt^3}{L}E\theta$$

The magnetic torque τ_M is given by the cross product of force with the lever arm l, integrated along the length of the filament

$$\tau_M = \int_0^L \vec{F} \times \vec{l}\ dl$$

If we assume a constant magnetic force along the length of the filament (i.e. B and ∇B are uniform along the length) which is applied in a direction perpendicular to the length, then the magnetic torque reduces to

$$\tau_M = \frac{1}{2}wtL^2\left(\frac{\chi}{\mu_0}B + M\right)\nabla B$$

Snap Condition

A tipping point occurs when the rate of change of magnetic torque is equal to the rate of change of elastic torque upon displacement, $d\tau_M/d\theta = d\tau_E/d\theta$. Using our expressions for elastic torque above, we find that the derivative is simply

$$\frac{d\tau_E}{d\theta} = \frac{1}{3}\frac{wt^3}{L}E$$

The derivative of magnetic torque is

$$\frac{d\tau_M}{d\theta} = L\frac{d\tau_M}{ds}$$

where *s* is in the direction of the displacement of the filament. Continuing with the derivative

$$\frac{d\tau_M}{d\theta} = \frac{1}{2}wtL^3\frac{d}{ds}\left(\frac{\chi}{\mu_0}B + M\right)\nabla B$$

$$\frac{d\tau_M}{d\theta} = \frac{1}{2}wtL^3\left[\left(\frac{\chi}{\mu_0}B + M\right)\frac{d}{ds}\nabla B + \nabla B\frac{d}{ds}\left(\frac{\chi}{\mu_0}B + M\right)\right]$$

$$\frac{d\tau_M}{d\theta} = \frac{1}{2}wtL^3\left[\left(\frac{\chi}{\mu_0}B + M\right)\frac{d(\nabla B)}{ds} + \nabla B\left(\frac{\chi}{\mu_0}\frac{dB}{ds} + \frac{dM}{ds}\right)\right]$$

$$\frac{d\tau_M}{d\theta} = \frac{1}{2}wtL^3\left[\left(\frac{\chi}{\mu_0}B + M\right)\frac{d(\nabla B)}{ds} + \nabla B\left(\frac{\chi}{\mu_0}\frac{dB}{ds} + \frac{dM}{dB}\frac{dB}{ds}\right)\right]$$

$$\frac{d\tau_M}{d\theta} = \frac{1}{2}wtL^3\left[\left(\frac{\chi}{\mu_0}B + M\right)\nabla^2 B + \nabla B\left(\frac{\chi}{\mu_0}\nabla B + \frac{\chi}{\mu_0}\nabla B\right)\right]$$

$$\frac{d\tau_M}{d\theta} = \frac{1}{2}wtL^3\left[\left(\frac{\chi}{\mu_0}B + M\right)\nabla^2 B + 2\frac{\chi}{\mu_0}(\nabla B)^2\right]$$

where ∇B and $\nabla^2 B$ indicate the magnetic field gradient and the first derivative of the magnetic field gradient in the direction of displacement. Here we have assumed that variations in χ with displacement are small. For low fields, where $\mu_0 M(B) = \chi B$, this further reduces to

$$\frac{d\tau_M}{d\theta} = wtL^3\frac{\chi}{\mu_0}\left[B\nabla^2 B + (\nabla B)^2\right]$$

Finally, from equating $d\tau_M/d\theta = d\tau_E/d\theta$, we find the tipping point condition

$$\frac{\chi}{\mu_0}\left[B\nabla^2 B + (\nabla B)^2\right] = \frac{Et^2}{3L^4}$$

In applied field geometries where the variation in magnetic field gradient is small $\left((\nabla B)^2 \ll B\nabla^2 B\right)$, this expression reduces further to

$$\frac{\chi}{\mu_0}(\nabla B)^2 = \frac{t^2}{3L^4}E$$

For the magnetic field geometries presented in this work, however, $(\nabla B)^2 \sim B\nabla^2 B$, so we have retained the additional term.

Quality

In the figure below, we have plotted the quality of actuation Q for our DiAPLEX cantilever as a function of magnetic field geometry (∇B,B) with L = 3 cm, t = 130 μm, E_H = 911 MPa (at 20° C), and E_L = 9 MPa (at 80° C), where and E_H and E_L are the highest and lowest elastic modulus available over the available temperature range, and $M(B)$ and $\chi(B)$ are provided above. The contours indicate Q, and regions with $Q < 0$ indicate failure due to either magnetic dominance (top-right) or elastic dominance (lower-left) across all temperatures.

Any path in the neighborhood of a magnet can be described as a single curve through this space. The black curve shown in **Figure S10** represents the field geometry along the axis of the permanent magnet used in cantilever experiments, where distances from the face of the magnet are noted. Using this figure, we can see that failure would occur for distances less than 11 mm or greater than about 30 mm, and the highest-quality switchability would occur at approximately 20 mm. The distance of 23 mm used in cantilever experiments, therefore, is quite close to optimal. This framework for calculating, plotting, and assessing Q could be readily extended to other shape memory polymers, magnetic particle loadings, or magnetic particle types, provided $E(T)$ and $M(B)$ are known.

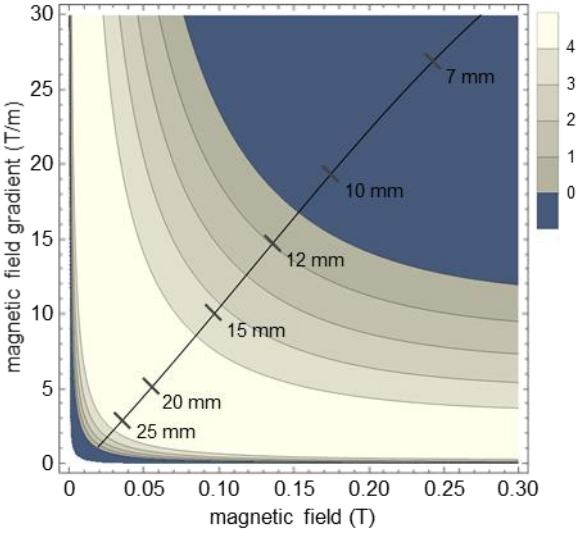

Fig. S10. Quality of actuation for a DiAPLEX cantilever as a function of magnetic field and field gradient. Contours represent the value of the quality of actuation Q, where higher Q represents higher quality switching between elastic and magnetic dominance upon heating of the shape memory polymer, and negative Q represents a failed actuator. The black curve indicates available field geometries along the axis of the 1-inch-diameter, 0.5-inch-thick cylindrical NdFeB magnet used in cantilever experiments, labeled with distances from the face of the magnet.